Role of infrared thermography in preoperative assessment of vascular access

by Giulia D'Ambrosio*, Giuseppe Gatta**, David Perpetuini*, Daniela Cardone*, Michele Tritto***, Francesco Aucella**, Maria Nardella**, Filippo Aucella**, Arcangelo Merla*

* *BioEngLab, Dipartimento di Ingegneria e Geologia, Università degli Studi G.d'Annunzio, Chieti-Pescara, Italy*

** *S.C. di Nefrologia e Dialisi, Fondazione IRCCS Casa Sollievo della Sofferenza, San Giovanni Rotondo, Italy*

*** *Next2U Srl, Pescara, Italy*

Abstract

Clinical infrared thermography provides a non-invasive functional assessment of hemodialysis vascular access and it is used to visualize superficial venous pathways, detect stenoses and evaluate distal perfusion through cooled-saline infusion. Building on this clinical framework, an automatic method is introduced to extract the cold-bolus trajectory from thermal video sequences. The method integrates arm tracking, differential-temperature enhancement, spatial and SNR-adaptive constraints, border-aware segmentation and branch selection to obtain vessel thermal-footprint width measurements over time. Applied to clinical cold-bolus sequences acquired during preoperative vascular-access assessment, the pipeline produces anatomically consistent vessel masks and a quantitative width-over-time profile.

1. Introduction

Infrared thermography is increasingly recognized as a non-invasive functional tool for evaluating hemodialysis vascular access. Since cutaneous temperature is strongly influenced by local blood perfusion, thermal maps provide indirect yet reliable information on superficial venous anatomy and hemodynamic alterations. In patients with arteriovenous fistulas (AVFs), thermographic images typically reveal hyperthermic patterns along arterialized veins and hypothermic regions associated with stenoses or distal ischemia.

A particularly powerful technique is *cold-bolus thermography*, in which cooled saline is infused distally to the planned anastomotic site, generating a propagating thermal front that renders superficial veins transiently visible as a negative ΔT contrast. This approach has been validated as a complement to Doppler ultrasound and digital phlebography across all phases of vascular access management [1], from preoperative mapping to postoperative surveillance of hemodialysis access-induced distal ischemia (HAIDI).

Despite its clinical promise, cold-bolus thermography currently relies exclusively on visual inspection of thermal sequences. Reproducibility is limited by inter-observer variability, and no quantitative descriptor of vessel morphology or bolus dynamics is extracted. Motion artefacts, and the time-varying nature of the ΔT contrast further complicate interpretation.

This paper presents an automatic pipeline for vessel segmentation in cold-bolus thermography. The method processes raw FLIR thermal sequences and produces, for each frame, a binary vessel mask and a quantitative vessel thermal-footprint width estimate. The contribution is threefold: (i) a hybrid Lucas–Kanade/GMM arm tracker with solidity-based quality control; (ii) an SNR-adaptive two-level thresholding scheme with a rolling-window spatial prior that handles the large variability in bolus contrast across subjects and frames; (iii) a distance-transform border exclusion that adapts dynamically to the arm silhouette at each frame.

The remainder of the paper is organized as follows. Section 2 reviews the clinical background of thermography in vascular access assessment. Section 3 describes the proposed pipeline in detail. Section 4 presents representative results, and Sections 5 and 6 provide discussion and conclusions.

2. Clinical Background

This section provides the clinical and technical context for the proposed method. Section 2.1 reviews the role of infrared thermography in vascular access assessment. Section 2.2 describes the cold-bolus technique and the physiological basis of the ΔT signal. Section 2.3 identifies the specific limitations of current qualitative approaches that motivate the development of an automatic segmentation framework.

2.1 Thermography in vascular access assessment

Clinical thermography is based on the detection of long-wave infrared radiation emitted by tissues at physiological temperatures. Because skin temperature is strongly influenced by local blood flow, thermographic maps provide indirect but reliable information on perfusion patterns [2, 3] and have historically been used to assess AVF function and detect flow abnormalities [4]. In patients with AVFs, thermal images typically show hyperthermic regions along the arterialized vein

License: https://creativecommons.org/licenses/by/4.0/deed.en

and hypothermic areas in regions affected by stenosis or distal ischemia [5, 6].

Figure 1 shows an example of a thermographic image of the upper limbs, where the limb bearing a distal AVF exhibits a clear hyperthermic pattern along the arterialized venous segment. Thermographic assessments are performed using a FLIR A500 thermal camera (resolution 464×348 px, thermal sensitivity $<$50 mK, spectral range 7.5–14 μm, frame rate up to 30 Hz) after a 30-minute acclimatization period in a temperature-controlled room (approximately 25 °C) [1].

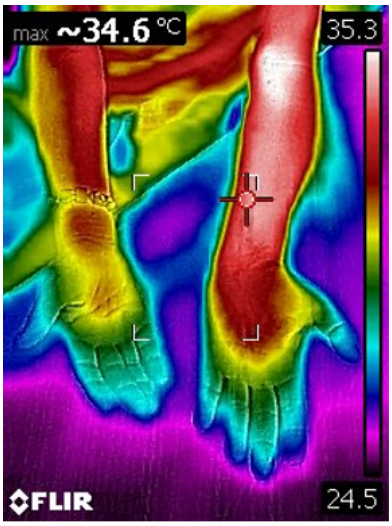

Fig. 1. *Static thermographic map of both upper limbs. Warmer regions (yellow–red) correspond to higher perfusion; cooler areas (blue–purple) indicate reduced distal perfusion.*

Thermography has been applied across multiple phases of vascular access management. In the *preoperative phase* it provides a panoramic overview of the limb, highlighting perfusion asymmetries that may indicate arterial insufficiency or venous abnormalities [7]. During *intraoperative procedures* it offers real-time feedback on perfusion changes at anastomosis (Fig. 2). In the *postoperative phase* it enables non-invasive monitoring of fistula maturation, detection of venous hypertension, and identification of HAIDI [8].

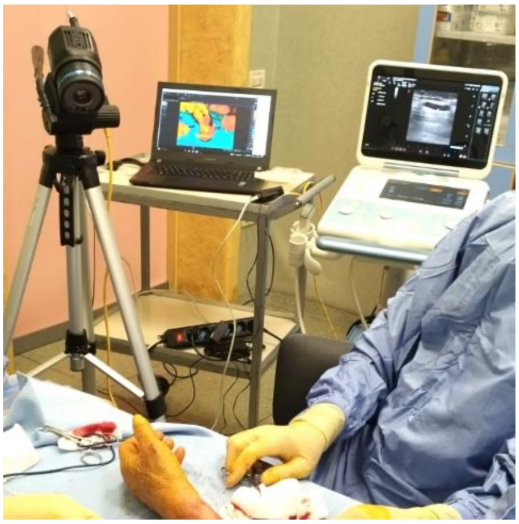

Fig. 2. *Intraoperative thermographic monitoring during AVF creation. Thermal patterns provide real-time feedback on perfusion changes [1].*

Despite these advantages, thermography is inherently limited to superficial structures: long-wave infrared radiation originates from the most superficial dermal layers, so deep or central veins remain invisible. Thermal patterns may

also be influenced by environmental conditions, patient movement, and camera artefacts, motivating the integration of thermography with computational methods capable of extracting reliable vessel information from dynamic thermal sequences.

2.2 Cold-bolus thermography

Among the extensions of clinical thermography, the infusion of cooled saline as a thermal contrast agent has proven particularly effective for rendering superficial veins transiently visible. This subsection describes the technique, its physical basis, and its validated clinical applications.

Infusing saline at approximately 15 ℃ at 20 ml/min through a 23 G needle cannula placed distally to the planned anastomotic site generates a transient negative thermal gradient that propagates along the venous pathway, becoming detectable within approximately 30 seconds of infusion onset, depending on vessel depth. Cold-bolus propagation can be described qualitatively by the transient heat equation:

$$\nabla^2 T - \frac{1}{\alpha}\frac{\partial T}{\partial t} = 0, \tag{1}$$

where α is the thermal diffusivity of tissue. Although biological perfusion introduces additional complexity, Eq. (1) captures the essential behavior of the cooling front as it travels along the vein.

Cold-bolus thermography has been validated against digital phlebography for superficial veins [9] and has demonstrated high sensitivity in identifying venous stenoses, accessory drainage pathways, flow diversion phenomena, and early HAIDI [1]. Dynamic thermal responses during post-occlusive reactive hyperemia (PORH) have also been shown to correlate with Doppler-derived resistance indices [10], supporting the physiological significance of the ΔT signal.

Several challenges arise when analyzing cold-bolus sequences automatically: the ΔT contrast is weak before bolus arrival and attenuates rapidly in deeper veins; wrist and forearm motion introduce spatial misalignment; and thermal noise may obscure thin vessel branches. These factors make manual interpretation difficult and motivate the automated pipeline described in Section 3.

2.3 Need for automatic vessel extraction

The clinical evidence reviewed above demonstrates the diagnostic value of cold-bolus thermography, but also highlights a critical gap: all existing analyses rely on qualitative visual interpretation. This subsection argues for the necessity of an automatic segmentation framework and defines the requirements it must satisfy.

Automatic segmentation of cold-bolus thermographic sequences remains an open problem [11]. Existing clinical studies rely on qualitative visual interpretation [1], which limits reproducibility and prevents quantitative characterization of vessel morphology or bolus dynamics. Existing thermographic vessel-segmentation methods address static imagery [6] and do not account for the combined challenges of motion compensation, time-varying contrast, and multi-branch venous topology encountered in dynamic cold-bolus sequences.

3. Proposed Segmentation Method

This section describes the automatic pipeline for vessel segmentation in cold-bolus thermography. The method is designed to operate on raw FLIR thermal sequences without manual vessel annotation and to address the three main challenges identified in Section 2: patient motion, time-varying ΔT contrast, and multi-branch venous topology. Vessel-detection thresholds are derived directly from the baseline noise distribution and from the frame-wise ΔT histogram, reducing dependence on fixed thermal values. The pipeline is presented first as a high-level overview (Section 3.1), followed by detailed descriptions of each functional stage (Sections 3.2–3.3).

3.1 Pipeline overview

The pipeline takes as input a sequence of calibrated temperature frames (units: °C) acquired during cold-bolus infusion and produces three outputs for each frame: (i) a conservative binary mask of the main vessel trunk, $M_{\text{trunk}}(x, y, t)$, (ii) a more permissive binary mask of the cooling venous tree, $M_{\text{tree}}(x, y, t)$, and (iii) a scalar thermal-width estimate $w(t)$ computed from the main trunk. A composite trajectory map is obtained as the union of the per-frame masks over the bolus propagation window.

Figure 3 provides a schematic overview of the full processing chain. The pipeline comprises six functional stages executed sequentially for each frame: ROI selection, baseline computation and differential-temperature (ΔT) mapping, motion compensation, adaptive vessel detection via data-driven adaptive thresholding, spatial continuity enforcement, and width measurement with outlier rejection. The first stage (ROI selection) requires a single manual operation performed once per sequence; all subsequent stages are fully automatic. The pipeline exposes only five user-facing parameters (Table 1); geometric constraints and detection thresholds are derived from the data at each frame and require no manual tuning. The core and side vessel thresholds are not fixed multiples of the local standard deviation, but are estimated from the empirical ΔT distribution using baseline noise modelling, Otsu thresholding, and a two-component GMM.

Fig. 3. *Schematic overview of the automatic cold-bolus vessel segmentation pipeline. Six sequential stages process each raw thermal frame to yield a conservative trunk mask M_{trunk}, a venous-tree mask M_{tree}, and a vessel thermal-footprint width estimate $w(t)$.*

Table 1. *User-facing parameters of the pipeline. All geometric constraints and thermal detection thresholds are derived automatically from the data at each frame.*

Parameter	Meaning	Default
s_{seg}	Vessel boundary expansion (0 = conservative, 1 = permissive)	0.50
s_{br}	Collateral branch retention (0 = trunk only, 1 = full venous tree)	0.50
α_{IIR}	Temporal smoothing strength (higher = more smoothing, slower response)	0.30
σ_G	Spatial smoothing scale (pixels)	1.0
N_{base}	Pre-bolus baseline window length	auto

3.2 Stages description

Baseline and ΔT computation. Before the cold bolus is injected, the first few seconds of the sequence are free of vascular signal and serve as a per-pixel thermal reference $T_0(x, y)$. Subtracting this baseline from each subsequent frame yields the differential map

$$\Delta T(x, y, t) = T_0(x, y) - T(x, y, t), \tag{2}$$

where positive values indicate pixels that have cooled relative to their pre-bolus state — and therefore candidate vein locations. The same baseline frames are used to characterise the intrinsic thermal noise of the sequence: the pipeline estimates the typical noise level from the data itself, so that any detection threshold applied later is automatically scaled to the actual noise floor of that recording rather than relying on a fixed value set in advance. Raw ΔT frames are then denoised by a two-stage filter cascade: a temporal IIR smoother that attenuates frame-level noise while preserving slow bolus dynamics [12]; and a spatial Gaussian filter that reduces pixel-level sensor noise. A short rolling-window temporal average is maintained in parallel to stabilise the ΔT signal in frames where the bolus contrast is temporarily weak [13].

Motion compensation. Patient motion causes frame-to-frame misalignment that can generate spurious cooling artefacts unrelated to the bolus. To track the arm robustly, the pipeline combines two complementary strategies at every frame: a Lucas–Kanade optical-flow estimator [14, 15] that follows smooth continuous motion by warping the previous arm mask, and a Gaussian mixture model (GMM) [16] that re-segments the arm from scratch based on the temperature histogram of the current frame. The two results are compared at each step; if they agree, the flow-based result is kept, otherwise the GMM result takes over. This handover mechanism makes tracking robust to both gradual drift and sudden repositioning, analogously to appearance-model-based tracking frameworks [17]. In a separate step it is computed, from the arm silhouette itself, how deep the exclusion zone around the arm boundary should be; this depth adapts automatically to the actual size and shape of the arm in each frame.

Adaptive detection. The core challenge of vessel detection in cold-bolus sequences is that the thermal contrast of the vein changes continuously as the bolus propagates, so a fixed detection threshold would either miss the vein in low-contrast frames or produce false positives in high-contrast ones [18]. Instead, at every frame the pipeline fits a two-component statistical model (GMM) to the ΔT values inside the arm, separating the background tissue distribution from the cooled-vein distribution. Otsu's method provides an independent estimate of the same boundary. The final detection

threshold τ_{core} is taken as the most conservative of the two data-driven estimates and the baseline noise floor:

$$\tau_{\text{core}}(t) = \max(\tau_{\text{Otsu}}(t),\ \tau_{\text{GMM}}(t),\ \tau_{\text{base}})\,. \tag{3}$$

Pixels exceeding τ_{core} form the high-confidence vessel nucleus. A second, slightly lower threshold — also derived from the current frame distribution and controlled by the sensitivity parameter s_{seg} — governs lateral widening: the nucleus skeleton is expanded perpendicularly to the vessel axis to recover the full vessel width, including the cooling halo around the vein wall. Collateral branches are retained when their thermal signal is sufficiently close to that of the main trunk, with the tolerance set by s_{br}, consistent with topology-aware segmentation approaches [19]. A local second-pass refinement repeats threshold estimation within a small neighbourhood of the first result as a consistency check.

Postprocessing. Between consecutive frames the detected vessel position is constrained to move by no more than a distance proportional to the arm width, preventing the tracker from jumping to unrelated cold artefacts. A late-drift correction monitors whether the vessel centroid has drifted away from its recent median position; if so, the previous frame's mask is propagated forward rather than accepting an implausible detection. Isolated blob-like regions — round, compact cold spots inconsistent with a tubular vessel — are automatically discarded, while elongated components connected to the main trunk are preserved to capture collateral drainage.

3.3 Vessel thermal-footprint width measurement

At each frame, the vessel width is measured on the conservative trunk mask using the mask skeleton and its Euclidean distance transform. Concretely, at every skeletal pixel the local half-width is read from the distance transform, and the final estimate is the median of these local measurements after discarding the most extreme values:

$$w(t) = \text{median}_{(x,y)\in S_t}[2\,D_{\text{trunk}}(x,y,t)]\,. \tag{4}$$

This skeleton-based approach [20] measures the thermal footprint of the main trunk independently of vessel length and branching, and is therefore more stable than area-based estimates. The raw width series is smoothed with a short median filter to suppress isolated outliers caused by momentary tracking failures, following the rationale of robust outlier rejection [21]. The resulting profile represents the apparent thermal width of the vein as seen by the camera; it can be related to the anatomical vessel diameter when pixel spacing and imaging geometry are calibrated, providing a quantitative complement to Doppler-derived measurements [22].

4. Results

The pipeline is applied to a representative cold-bolus thermographic sequence of 2551 frames acquired during preoperative vascular-access assessment. Results are reported both visually and through an internal quality-control analysis designed to identify the temporal interval in which the bolus signal remained spatially localized and suitable for quantitative processing. Figure 4 shows a representative frame within the accepted bolus-propagation window. The cooling front is visible as a negative thermal contrast along the superficial venous pathway, and the conservative trunk mask remains spatially aligned with the main vessel. The extracted contour captures the dominant venous trunk while avoiding the warmer arm borders and background regions.

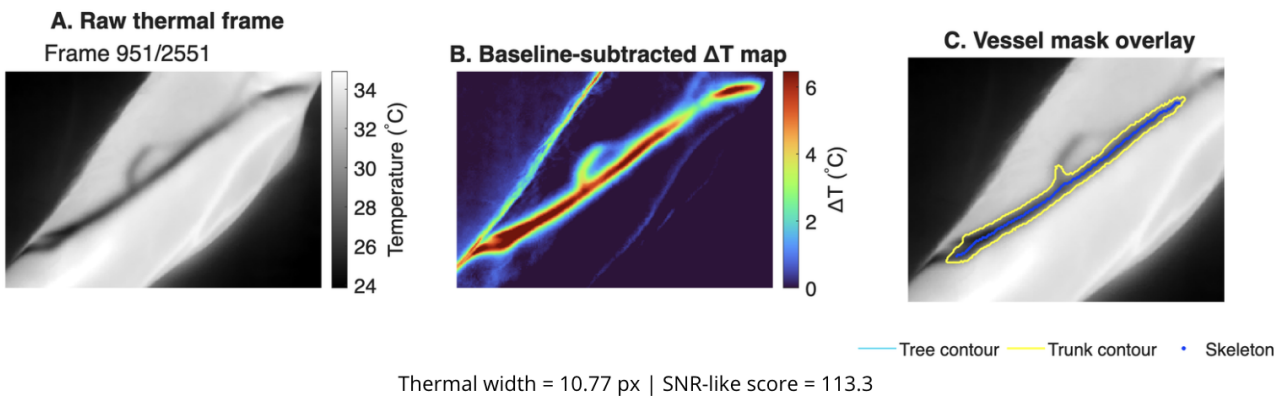

Fig. 4. *Representative cold-bolus frame (frame 951/2551) within the quality-controlled analysis window.* ***A****: raw thermal frame.* ***B****: baseline-subtracted ΔT map.* ***C****: vessel mask overlay with venous-tree contour (cyan), trunk contour (yellow), and skeleton (blue dots). Thermal width = 10.77 px; SNR-like score = 113.3.*

Figure 5 shows the quality-controlled composite trajectory map, obtained by accumulating only the venous-tree masks that passed the internal quality-control criteria. This avoids including late frames in which the cooling pattern becomes diffuse and may lead to mask overgrowth. The resulting trajectory is anatomically consistent with the superficial venous pathway visible in the thermal sequence and preserves the main trunk together with the thermally supported collateral branch.

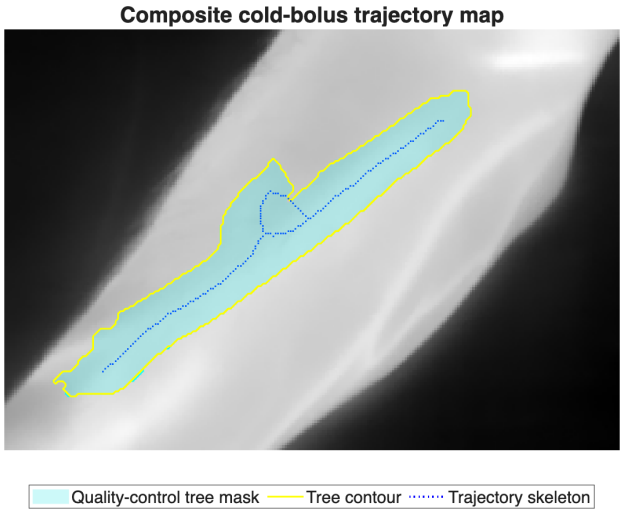

Fig. 5. *Quality-controlled (QC) composite cold-bolus trajectory map overlaid on the baseline thermal image. The cyan area represents the accumulated venous-tree mask, the yellow contour its external boundary, and the blue dotted line the extracted trajectory skeleton.*

Figure 6 reports the thermal-width profile and the corresponding thermal signal quality. The accepted quality-controlled bolus window extended from frame 93 to frame 1893. Frames outside this interval are retained for visual inspection but excluded from quantitative width estimation because the late cooling pattern became more diffuse and produced occasional unstable width values.

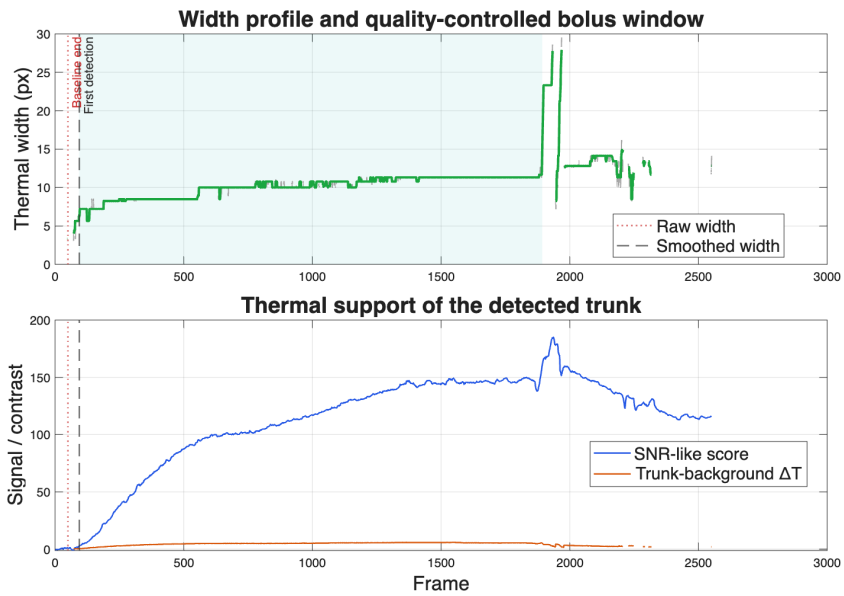

Fig. 6. *Quality-control (QC) summary of the extracted thermal-width profile. The upper panel reports raw and filtered width values, with the accepted bolus-analysis window highlighted. The lower panel reports the local thermal signal quality and the trunk-to-background thermal contrast over time.*

The internal quality-control analysis showed low pre-bolus false-positive activity, with vessel detections in 2 out of 50 baseline frames (4.0%). After bolus arrival, a valid trunk mask is obtained in 87.3% of post-baseline frames, while the quality-controlled analysis retained 71.6% of post-baseline frames. The first reliable detection occurred at frame 94. Within the accepted window, spatial tracking is stable, with a median centroid displacement of 0.08 px/frame and a 95th percentile displacement of 0.42 px/frame. The median apparent thermal width of the main trunk is 10.48 px (instantaneous value at the representative frame: 10.77 px), with a robust standard deviation of 1.23 px. The median trunk-to-background thermal contrast is 5.14 °C, and the 25th percentile remained 4.77 °C, confirming that the segmented region corresponded to a strong and persistent cooling signal. No trunk-tree inconsistency is observed, indicating that the conservative trunk mask remained fully contained within the venous-tree mask. The quality-controlled composite trajectory covered an area of 4610 px and had a skeleton length of 171 px. These descriptors provide compact quantitative summaries of the thermographically visible venous pathway and may support the qualitative interpretation of cold-bolus propagation.

5. Discussion

This work presents an automatic segmentation framework for cold-bolus thermography applied to the preoperative assessment of hemodialysis vascular access. Building on the clinical framework described in [1], the proposed method translates a qualitative dynamic thermographic examination into a reproducible quantitative analysis of venous trajectory and apparent thermal width. From a clinical perspective, cold-bolus thermography is valuable because it provides a non-invasive and panoramic visualization of superficial venous pathways using cooled saline as a functional contrast agent; as reported in [1], this approach can complement Doppler ultrasound and digital phlebography by helping to identify the course of candidate veins, collateral drainage pathways, stenotic interruptions, and perfusion alterations relevant to vascular-access planning and surveillance. The automatic pipeline proposed here addresses one of the current limitations of this technique—the dependence on visual interpretation of thermal videos—through a six-stage architecture designed to mitigate the main technical sources of variability encountered in cold-bolus sequences. The hybrid LK/GMM arm tracker handles both smooth continuous motion and sudden repositioning: the LK stage provides efficient frame-to-frame alignment, while the GMM re-segmentation offers a frame-independent fallback when the flow estimate drifts, a complementary design analogous to appearance-model-based tracking frameworks [17]. The two-stage ΔT filtering separates temporal frame noise, spatial sensor noise, and spike artefacts, following established practice in infrared sequence processing [12], while the thresholding stage reduces empirical tuning by estimating vessel thresholds from the frame-wise ΔT distribution and from the baseline noise model rather than relying on fixed thermal thresholds. Finally, the distance-transform border exclusion suppresses systematic edge artefacts while adapting to the actual arm geometry at each frame.

The quality-control analysis is essential for separating the clinically interpretable bolus-propagation interval from late frames affected by diffuse cooling. Within the accepted window, the low centroid drift, high thermal contrast, and absence of trunk-tree inconsistencies indicate that the detected mask is spatially stable, thermally supported, and topologically coherent. The apparent thermal-width profile should not be interpreted as a direct anatomical vessel diameter unless pixel spacing, viewing geometry, and vessel depth are calibrated. However, it provides a reproducible descriptor of the thermal footprint of the main venous trunk and may complement Doppler-derived diameter measurements when appropriate calibration is available [22].

Several limitations should be acknowledged. Although the pipeline reduces the most important fixed thermal thresholds, it remains a classical rule-based segmentation framework with technical guardrails for tracking, shape selection, temporal smoothing, and drift correction. The current validation is an internal quality-control analysis rather than a ground-truth segmentation benchmark. Ground-truth annotation of dynamic cold-bolus sequences is inherently challenging: the vessel boundary in the ΔT domain shifts continuously with bolus propagation, and manual frame-by-frame delineation would reintroduce the inter-observer variability that the proposed framework aims to overcome. Comparison against phlebographic and Doppler reference data therefore represents a more meaningful validation target, and future prospective studies should pursue this direction. Furthermore, the method is inherently limited to superficial vessels, consistent with the physical constraints of infrared thermography. The manual ROI selection step introduces residual operator dependency, and future versions should include automatic limb detection. Finally, although the current implementation separates trunk and tree masks, it does not yet produce an explicit graph representation of venous topology; a graph-based centreline extraction approach [23] could provide this information.

6. Conclusion

This study demonstrates the feasibility of automatic vessel extraction from cold-bolus infrared thermography sequences acquired during preoperative vascular-access assessment. The proposed pipeline combines hybrid Lucas–Kanade/GMM arm tracking, distance-transform border exclusion, two-stage differential-temperature filtering, data-driven adaptive thresholding based on baseline noise and frame-wise Otsu/GMM modelling, topology-aware branch handling, and robust width measurement on the main venous trunk.

The results support the role of thermography as a non-invasive, panoramic, and functional complement to existing diagnostic tools in vascular access management [1]. By automatically extracting the cold-bolus trajectory and a thermal-width profile, the method introduces quantitative descriptors that can help document superficial venous pathways, collateral

drainage, and potential flow interruptions—features that are currently evaluated mainly through visual inspection. Rather than replacing Doppler ultrasound or phlebography, this approach enhances the clinical utility of cold-bolus thermography by making its interpretation more reproducible and suitable for post-processing. Future developments will focus on prospective validation against phlebographic and ultrasound reference data, quantitative benchmarking of segmentation accuracy, graph-based analysis of venous branching, and the possible integration of deep-learning-based vessel enhancement [24] to improve sensitivity in low-contrast frames.

Acknowledgments

This work was supported by the National Centre for High Performance Computing, Big Data and Quantum Computing (CN HPC), Spoke 6, under the Public Call for Collaborative Research and Development Projects, Project ID 0008, entitled “In silico trial of skin thermal profile for pulse wave stratification: A multiphysics and machine-learning approach”. The authors gratefully acknowledge the financial support provided within the framework of Italy’s National Recovery and Resilience Plan (PNRR), funded by the European Union – NextGenerationEU.

References

[1] Giuseppe Gatta, Antonio Scarlatella, Francesco Aucella, Maria Nardella, David Perpetuini, Michele Tritto, Daniela Cardone, Carlo Lomonte, Arcangelo Merla, and Filippo Aucella. Utilità della termografia nella diagnostica degli accessi vascolari per emodialisi. *Giornale Italiano di Nefrologia*, 41(4), 2024.

[2] Giovanni Piva, Anna Crepaldi, Gladiol Zenunaj, Lorenzo Caruso, Natascia Rinaldo, VIncenzo Gasbarro, Nicola Lamberti, Pablo López-Soto Jesús, and Fabio Manfredini. The value of infrared thermography to assess foot and limb perfusion in relation to medical, surgical, exercise or pharmacological interventions in peripheral artery disease: A systematic review. *Diagnostics*, 12(12):3007, 2022.

[3] David Perpetuini, Chiara Filippini, Michele Zito, Daniela Cardone, and Arcangelo Merla. Altered microcirculation in alzheimer’s disease assessed by machine learning applied to functional thermal imaging data. *Bioengineering*, 9(10):492, 2022.

[4] John Allen, Crispian P Oates, Ahmed D Chishti, Ihab A M Ahmed, David Talbot, and Alan Murray. Thermography and colour duplex ultrasound assessments of arteriovenous fistula function in renal patients. *Physiological Measurement*, 27:51–60, 2006.

[5] J P Masselot, J P Adhémar, J Laederich, and D Kleinknecht. Thermography: an alternative to angiography for vascular access survey in haemodialysis. *Proceedings of the European Dialysis and Transplant Association*, 16:272–276, 1979.

[6] Julien Al Shakarchi, Steve Mellor, and Nicholas Inston. The novel use of infrared thermal imaging as an adjunct for the management of haemodialysis access induced distal ischemia. *Journal of Vascular Access*, 17(4):e70–2, 2016.

[7] Marko Malovrh. Native arteriovenous fistula: preoperative evaluation. *American Journal of Kidney Diseases*, 39(6):1218–25, 2002.

[8] Gregor Novljan, Rina R Rus, Anja Koren-Jeverica, Tadej Avčin, Rafael Ponikvar, and Jadranka Buturović-Ponikvar. Detection of dialysis access induced limb ischemia by infrared thermography in children. *Therapeutic Apheresis and Dialysis*, 15(3):298–305, 2011.

[9] Tomas V Gonzales, Candice A Bookwalter, Thomas A Foley, and Prabhakar Shantha Rajiah. Multimodality imaging evaluation of arteriovenous fistulas and grafts: a clinical practice review. *Cardiovascular Diagnosis and Therapy*, 13(1):196–211, 2023.

[10] David Perpetuini, Michele Tritto, Daniela Cardone, Giuseppe Gatta, Antonio Scarlatella, Maria Nardella, Francesco Napolitano, and Arcangelo Merla. Preliminary findings on the use of infrared thermal imaging for the detection of reactive hyperemia in the upper limb on vasculopathic patients. *Engineering Proceedings*, 51(1):3, 2023.

[11] Ling Li, Haoting Liu, Qing Li, Zhen Tian, Yaije Li, Wenjia Geng, and Song Wang. Near-infrared blood vessel image segmentation using background subtraction and improved mathematical morphology. *Bioengineering*, 10(6):726, 2023.

[12] Gilbert Gaussorgues. *La thermographie infrarouge: principes, technologies, applications*. Lavoisier, Paris, France, 4 edition, 1994.

[13] Richard B Buxton. *Introduction to Functional Magnetic Resonance Imaging: Principles and Techniques*. Cambridge University Press, Cambridge, UK, 2002.

[14] Bruce D Lucas and Takeo Kanade. An iterative image registration technique with an application to stereo vision. In *Proceedings of the 7th International Joint Conference on Artificial Intelligence (IJCAI)*, volume 2, pages 674–679, 1981.

[15] Zachary Teed and Jia Deng. Raft: Recurrent all-pairs field transforms for optical flow. *CoRR*, abs/2003.12039, 2020.

[16] Douglas A Reynolds. Gaussian mixture models. In Stan Z. Li and Anil Jain, editors, *Encyclopedia of Biometrics*, pages 659–663. Springer, Boston, MA, 2009.

[17] Dorin Comaniciu, Visvanathan Ramesh, and Peter Meer. Kernel-based object tracking. *IEEE Transactions on Pattern Analysis and Machine Intelligence*, 25(5):564–577, 2003.

[18] Chang Liu, Fengying Xie, Xiaomeng Dong, Hongxia Gao, and Haopeng Zhang. Small target detection from infrared remote sensing images using local adaptive thresholding. *IEEE Journal of Selected Topics in Applied Earth Observations and Remote Sensing*, 15:1941–1952, 2022.

[19] Xiaowei Liu, yikun Hu, Jianguo Chen, and Keqin Li. Shape and boundary-aware multi-branch model for semi-supervised medical image segmentation. *Computers in Biology and Medicine*, 143:105252, 2022.

[20] Robert M Haralick and Linda G Shapiro. *Computer and Robot Vision*, volume 1. Addison-Wesley, Reading, MA, 1992.

[21] Ronad K Pearson. Outliers in process modeling and identification. *IEEE Transactions on Control Systems Technology*, 10(1):55–63, 2002.

[22] Magnus Cinthio, Tomas Jansson, Åsa Rydén Ahlgren, Kjell Lindström, and Hans W Persson. A method for arterial diameter change measurements using ultrasonic b-mode data. *Ultrasound in Medicine and Biology*, 36(9):1504–1512, 2010.

[23] Alejandro F Frangi, Wiro J Niessen, Koen L Vincken, and Max A Viergever. Multiscale vessel enhancement filtering. In *Medical Image Computing and Computer-Assisted Intervention (MICCAI)*, pages 130–137, Berlin, Heidelberg, 1998. Springer.

[24] Olaf Ronneberger, Philipp Fischer, and Thomas Brox. U-net: Convolutional networks for biomedical image segmentation. In *Medical Image Computing and Computer-Assisted Intervention (MICCAI)*, pages 234–241. Springer, 2015.